

Article

An Attractive Blue Diopside from Sissone Valley, Western Alps, Italy

Franca Caucia ^{1,*}, Maurizio Scacchetti ¹, Luigi Marinoni ¹, Mattia Gilio ¹ , Antonio Langone ², Omar Bartoli ³, Marco Vanotti ¹ and Ivano Foianini ¹

¹ Earth and Environmental Sciences Department, University of Pavia, Via Ferrata 1, 27100 Pavia, Italy; mauscacchetti@alice.it (M.S.); luigitito.marinoni@unipv.it (L.M.); mattia.gilio@unipv.it (M.G.); marco.vanotti@gmail.com (M.V.); ifoianini@fondazionefoianini.it (I.F.)

² IGG-Geosciences and Earth Resources Institute CNR, Via Ferrata 1, 27100 Pavia, Italy; langone@igg.cnr.it

³ Geosciences Department, University of Padova, Via Gradenigo 6, 35100 Padova, Italy; omar.bartoli@unipd.it

* Correspondence: caucia@crystal.unipv.it

Abstract: In this work a rare and attractive blue diopside present in Sissone valley in the Western Alps was investigated through different methodologies: geological survey; standard gemological methods; X-Ray Powder Diffraction; SEM observations; Raman spectrometry; EMP analyses of major elements; and LA-ICP-MS analyses for minor and trace elements. The host rock of investigated gems is represented by a Mg-calcite bearing marble, belonging to the Suretta nappe and composed of blue diopside, lizardite, phlogopite, forsterite, Ca-Mg-amphibole, and thomsonite; the rock was metamorphosed by the intrusion of Masino-Bregaglia pluton. The diopside is generally found in the core of veins in contact with green–blue tremolite and, more externally, with green–yellowish lizardite. The diopside samples show opaque diaphaneity, are inert to long and short-waves UV radiation, and their specific density varies between 3.24 and 3.30 g/cm³ while medium refraction between 1.680–1.683. The diopside shows a polycrystalline texture with interstitial Mg-calcite which acts as binder. The characteristic blue–turquoise color is mainly determined by traces of V and subordinately of Fe, Mn, Cr and Ti. The contents of V and Ti show a good positive correlation. The minerals associated with diopside in the lenticular veins also show enrichments in V. The blue diopside of the Sissone valley could certainly present a good commercial value, but unfortunately it is difficult to reach the outcrop sites.

Keywords: diopside; LA-ICP-MS; Sissone valley; blue gemstone; chromophore elements; Raman spectroscopy



Citation: Caucia, F.; Scacchetti, M.; Marinoni, L.; Gilio, M.; Langone, A.; Bartoli, O.; Vanotti, M.; Foianini, I. An Attractive Blue Diopside from Sissone Valley, Western Alps, Italy. *Minerals* **2021**, *11*, 837. <https://doi.org/10.3390/min11080837>

Academic Editors: Thomas Hainschwang and Frederick Lin Sutherland

Received: 31 May 2021

Accepted: 26 July 2021

Published: 1 August 2021

Publisher's Note: MDPI stays neutral with regard to jurisdictional claims in published maps and institutional affiliations.



Copyright: © 2021 by the authors. Licensee MDPI, Basel, Switzerland. This article is an open access article distributed under the terms and conditions of the Creative Commons Attribution (CC BY) license (<https://creativecommons.org/licenses/by/4.0/>).

1. Introduction

Diopside is a Ca and Mg silicate with formula $\text{CaMg}(\text{Si}_2\text{O}_6)$ belonging to the pyroxene group. This mineral is generally found in the form of prismatic crystals with a square or octagonal rectangular section or also as granular or fibrous-radial aggregates of light green, blue, whitish, yellowish or dark brown color. It has a Mohs hardness between 5.5 and 6.5; it is fragile and perfectly flaked according to the two orthogonal planes [100] and [010]. Diopside generally occurs in several contact-metamorphic rocks such as metamorphosed siliceous limestones, dolomites and skarns, in ultramafic igneous rocks such as kimberlites, peridotites, and also rodingites [1–3]. Diopside also occurs in basic-ultrabasic rocks as picritic lava [4] and basaltic lava [5].

Diopside has been already considered a gem since ancient times; its name derives from the Greek words “di” (for “two” or “double”) and “opsis” (“look”), probably referring to its properties of birefringence or pleochroism. In the gem-quality varieties, diopside shows a diaphaneity varying from transparent to translucent and vitreous luster. The most important chromophore elements of the gem-quality diopside are Cr and Fe, which give

the mineral different shades of green, and V, Mn and Ti, which are generally responsible for the blue varieties [6].

Gem-quality diopside is mined in several countries; the most famous varieties are the “black star”, the “Cr-diopside” and the “violane”. “Black star” diopside comes from India; its name is due to the black or greenish-black color and to the optical phenomenon of “asterism”, which is a four-rayed star visible on the surface of the cabochon gem. This effect is due to the presence of magnetite needles. The beautiful star diopsides inspired the imagination of the ancient Greeks, who believed they were small bright stars that turned to stone when they fell to Earth (Figure 1).

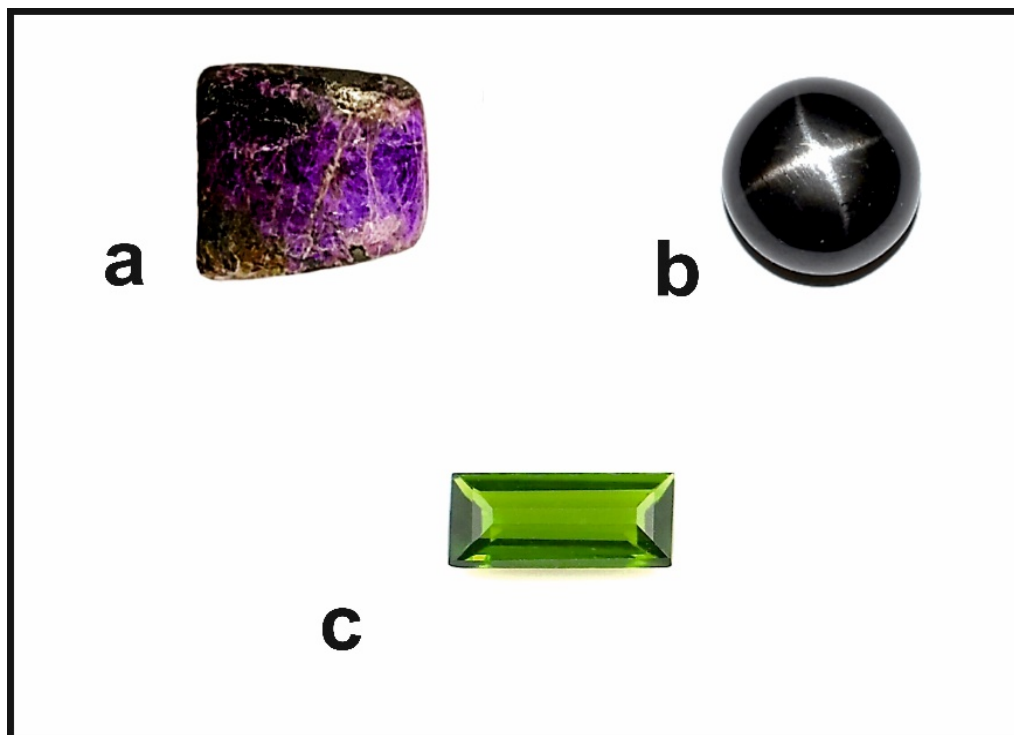


Figure 1. Photographs of some gem-quality diopsides: (a) “violane” (Praborna mine, Valle d’Aosta, Italy; 16 mm × 9 mm × 7 mm); (b) “black star” (Queensland, Australia; 10 mm × 7 mm); (c) Cr-diopside (Yakutia, Russia; 11 mm × 6 mm × 4 mm). Private collection of the author F.C. Photo Franca Caucia.

Cr-diopside is characterized by an intense green color, sometimes with bluish shades, due to the presence of Cr. It is commonly mined in the Yakutia region of Russia, while the light green variety, with the trade name of “tashmarine”, comes from the Tien Shan mountain range in the Xinjian region of China. “Violane” is a variety of diopside rich in manganese, extracted mainly from the Praborna manganese mine near St. Marcel in Aosta Valley (Italy). It is a very rare mineral with a color ranging from violet to bluish purple to lilac, depending on the content of the chromophore elements, which are mainly the Mn^{2+} , Mn^{3+} , Fe^{2+} , V^{4+} and Ti^{4+} ions [1–3,7].

In this work, some diopside samples from the upper Sissone valley, showing an unusual blue color were analyzed to evaluate their gemological relevance, to identify the chromophores responsible for color and to investigate the genetic conditions. This diopside is highly appreciated by collectors and numerous specimens are exhibited in local museums. The Sissone valley has been the subject of various scientific research projects due to the presence of numerous sites of petrological, mineralogical and gemological interest.

2. Geological Background

The Sissone valley is located in the north-western part of Malenco valley, which is considered one of the most interesting areas in Italy for studying the structure of the Alpine

chain and its geodynamic evolution [8–10]. The overall geosubstructural framework of the region is characterized by a series of thrust nappes with a sub-horizontal orientation and thicknesses ranging from a few hundred to a few thousand meters. From the bottom to the top, these nappes overlap according to the following sequence: Suretta, Forno and Malenco, Margna, Sella, Bernina, medium–upper Austroalpine units [11]. In the north-western part of the Malenco valley, and in Sissone valley, the sequence of nappes is interrupted by the late-alpine intrusion of the granodioritic and quartzdioritic Masino-Bregaglia massif (Figure 2). This massif is mainly composed of granodiorite (“Ghiandone”) with glandular facies and orthoclase megacrystals, immersed in a medium grain size matrix consisting of K-feldspar, plagioclase, quartz, biotite, hornblende, and accessories [12].

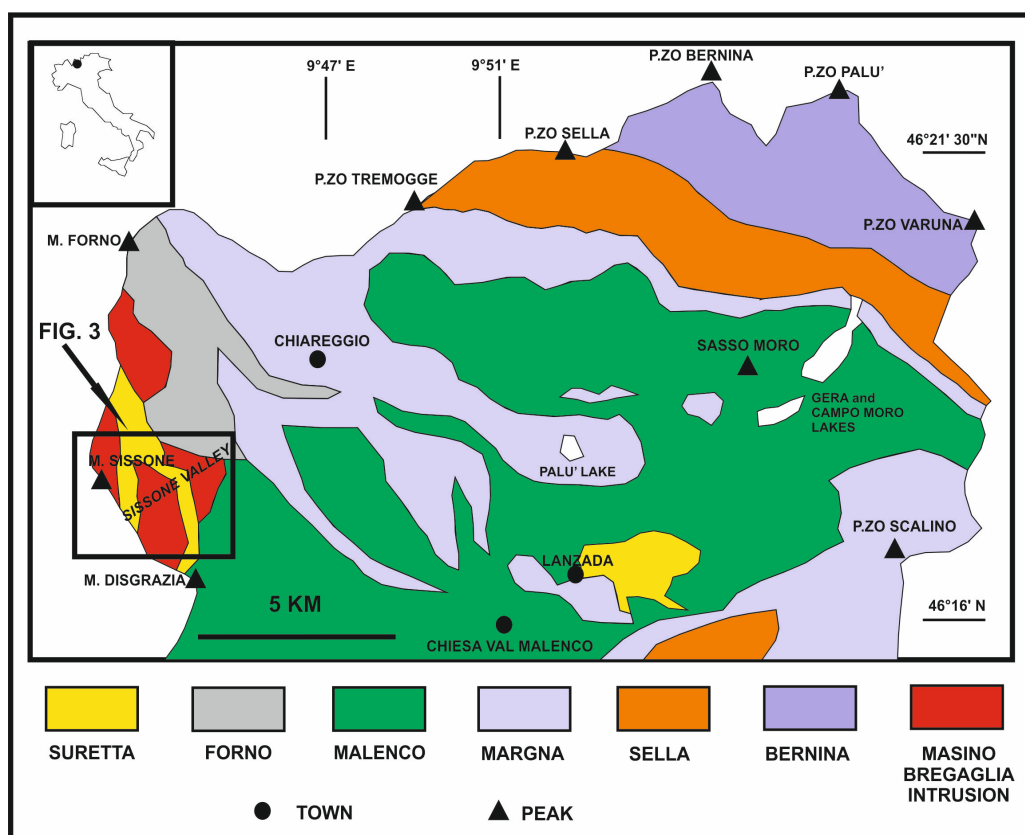


Figure 2. Tectonic map with the nappes of Malenco valley. Every nappe is composed by a Paleozoic crystalline basement and a Permo-Mesozoic sedimentary cover. The Masino-Bregaglia intrusion is dated to the Cenozoic Era. Map redrawn from [13].

The quartzdiorite (“Serizzo”) outcrops are present in the most marginal parts of the pluton and are therefore more abundant in Sissone valley; Serizzo is a rock with variable schistosity, with tonalitic facies, and composed of hornblende, biotite, plagioclase and subordinated quartz, K-feldspar, chlorite, epidote, titanite and accessory minerals [13]. The swarms of aplitic–pegmatitic felsic dykes cut through both plutonic and host rocks and represent the most recent expression of the entire Late Alpine magmatic cycle (Figure 3).

The contact aureole of Masino-Bregaglia pluton includes numerous levels of Mesozoic carbonate rocks pertaining to the Suretta Nappe, and outcrops are especially noticeable between the Vazzeda peak and the Sissone and Disgrazia glaciers. Furthermore, marble blocks of various dimensions are included by intrusive rocks as roof pendants [14]. The metamorphosed carbonate rocks are of two types: calcite marbles with oxides or Mg-silicates and marbles with Ca-oxides and calciphyres [13].

These metacarbonate rocks were formed under high temperature conditions during and shortly after the intrusion of Masino-Bregaglia pluton and are made up of different

and often mixed mineralogical parageneses: the most common is the association of calcite with Ca-silicates such as grossular, vesuvianite, epidote and wollastonite [13]. Within these marbles, concentrically zonate lenses of up to 20 cm thick occur, made up of finely granular blue–turquoise diopside mixed with colorless diopside and surrounded by fibrous tremolite and green diopside (Figure 4) [15–17].

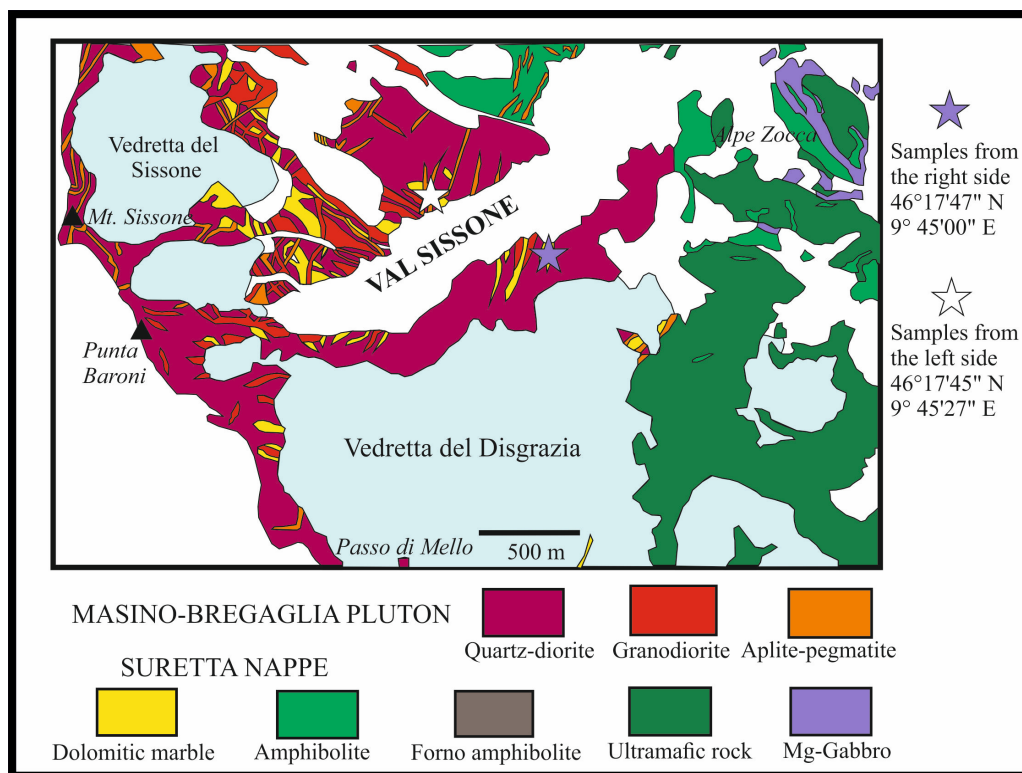


Figure 3. Geological map of the Sissone valley, with the location of the studied specimens (stars). Map redrawn from [14].

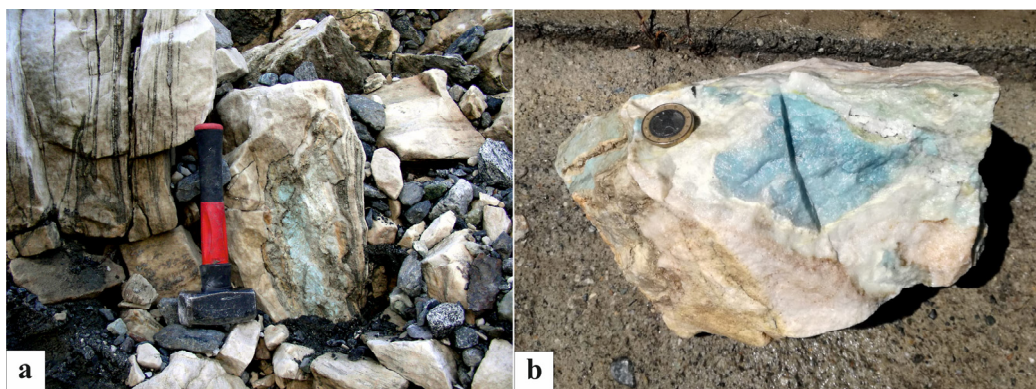


Figure 4. (a) Erratic pebble from the right side of the Sissone valley; (b) sample of marble lens showing the blue diopside in the core and the rims of white tremolite.

The samples investigated in the present paper belong to this paragenesis and come from two different areas of the valley, as shown in Figure 3. The first group of samples was extracted from an erratic boulder on the left side of the valley (*Uralite’s plain*) and was kindly offered by Mr. Pietro Nana [18]. The erratic boulder is located on a moraine shelf at an altitude of 1950 m, near the path that leads to the Sissone Alps (Figure 5).

The block, of metric dimensions, is made up of marble and includes a turquoise vein that immediately attracted the attention of mineral collectors. During the 1960s, the mineral

collector Mr. Francesco Bedognè was the first to extract from this boulder some samples of considerable mineralogical interest, which are now exhibited in the museums of Valtellina. The boulder is located at the edge of the moraine and this suggests that it was released by the “Vedretta del Sissone” glacier during its retreat at the end of the Little Ice Age (late 1800s). Alternatively, it might derive from a landslide or from the disintegration of some marble lenses present on the same side of the valley, at the foot of Cime di Rosso, Vazzeda and Sissone peaks. In fact, inside some landslide deposits located a few hundreds of meters downstream of the boulder, there are blocks of predominantly green diopside, once called “uralite” and considered pseudomorphoses of amphibole on pyroxene. “Uralite” is actually an iron diopside with traces of aluminum, manganese and sodium; it often occurs in association with epidote–clinozoisite and pyrite cubes. The other samples were collected by one of the authors (Ivano Foianini) from rocky outcrops on the right side of the valley.

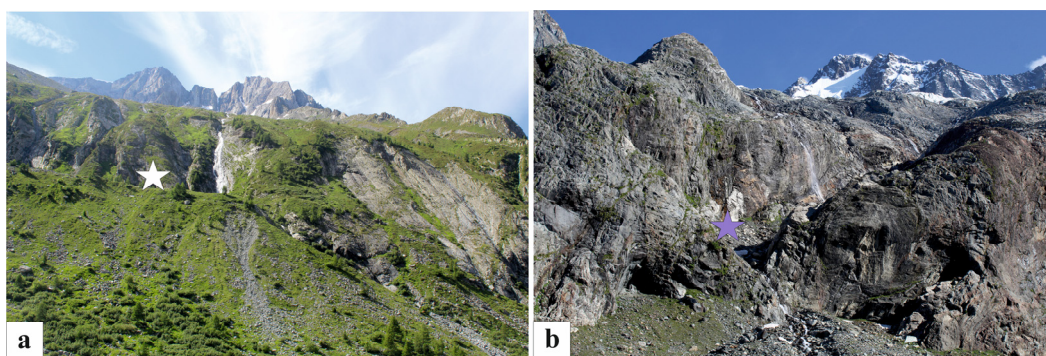


Figure 5. (a) Overviews of the left side (a) and right side (b) of the Sissone valley, with the locations of the investigated samples (stars).

Both samples could have the same origin and then could have been deposited by glaciers on the two sides of the valley. However, the marble lenses may have originally been present on both sides of the valley.

3. Materials and Methods

The mineralogical analyzes were carried out on the samples collected both on the right (outcrop rock) and on the left side (erratic boulder) of the Sissone valley. All the specimens were analyzed by X-ray powder diffraction (XRPD), Raman spectroscopy, laser ablation inductively coupled plasma mass spectrometry (LA-ICP-MS), and classic gemological analyses. The investigated blue diopsides were polished and reduced in splinters or small pebbles. Some of these were then chosen for their color (one of each tonality) and cut (cabochon cut with different shapes: Figure 6a,b, Figure 7a,b and Figure 8).

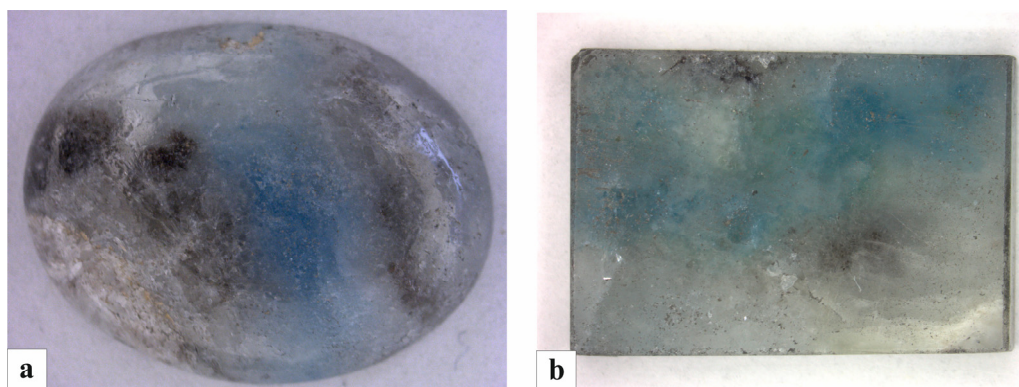


Figure 6. Fashioned gems with blue diopside (samples from the right side of the Sissone valley): (a) sample 9: cabochon cut, oval shape, dimensions 18 mm × 15 mm × 4 mm (photo by E. Borghi); (b) sample 6: fantasy cut rectangular shape, dimensions 15 mm × 10 mm × 2 mm.

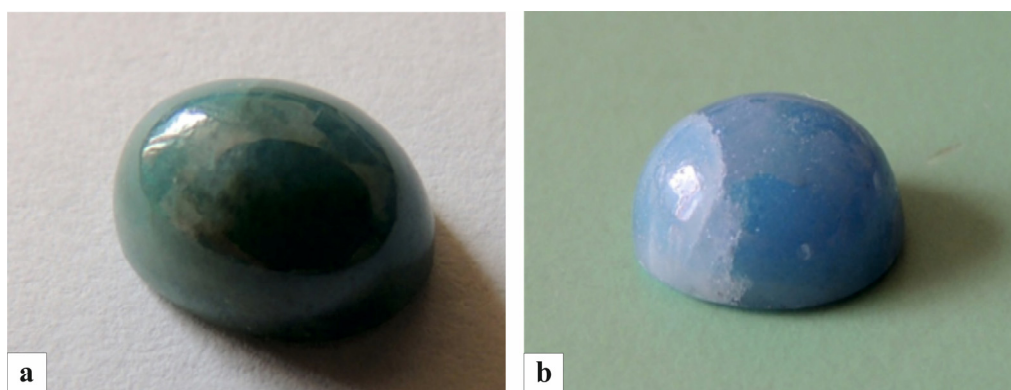


Figure 7. Cabochon-cut gem samples 1 (a) and 2 (b), from the left side of the Sissone valley. Dimensions: (a) 7 mm × 10 mm × 5 mm; (b) 7 mm × 9 mm × 5 mm.

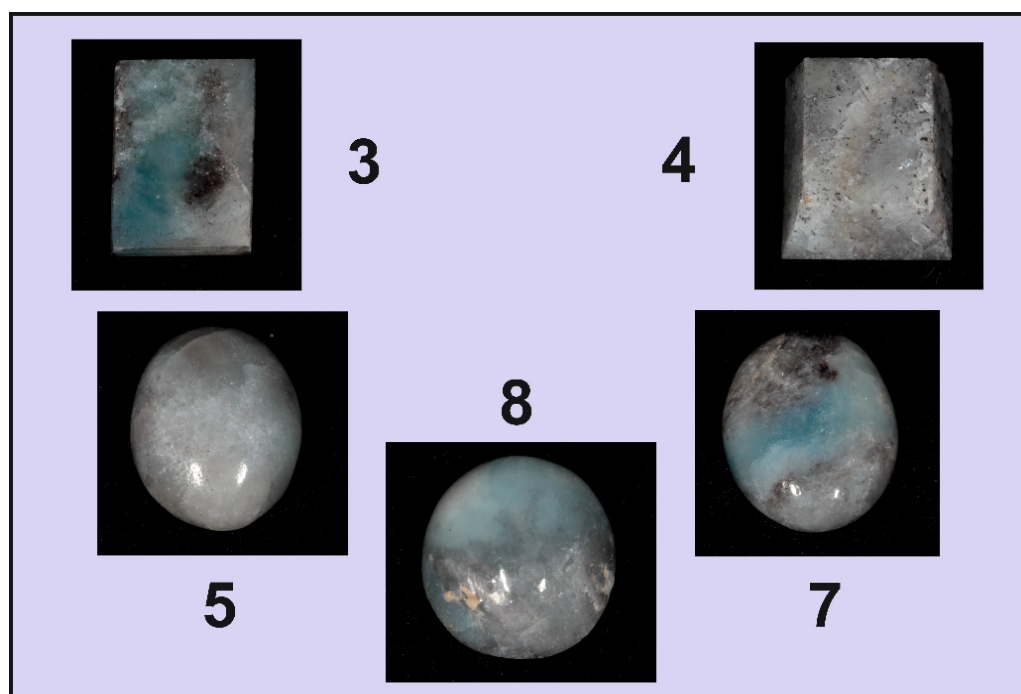


Figure 8. Another five cabochon-cut gems analyzed in this work, from the right side of the valley; samples 3 (14 mm × 11 mm × 5 mm); 4 (13 mm × 11 mm × 4 mm); 5 (17 mm × 13 mm × 4 mm); 7 (13 mm × 10 mm × 4 mm); 8 (19 mm × 14 mm × 6 mm).

The cabochon-cut diopside was examined through standard gemological methods to determining its optical properties, hydrostatic specific density (SD), UV fluorescence and microscopic features. The refractive indices (RI) were measured by the distance method with a Kruss Refractometer (A.Kruss Oftronic, Hamburg, Germany) (1.45–1.80 range) using ordinary light source with a sodium filter (589 nm) and methylene iodide as contact liquid ($n = 1.80$). A Mettler hydrostatic balance (GEMMARUM, Cavalese, Italy) was used to determine the specific density in bi-distilled water. The ultraviolet fluorescence was investigated both in short (254 nm) and long (366 nm) wavelength ultraviolet light, using a Wood lamp (GEMMARUM, Cavalese, Italy). The color was determined with a RGB Color System; all diopside crystals are polychrome. The physical and gemological properties of the blue diopside are reported in Table 1.

Table 1. Physical and gemological properties of the studied samples. Lsb = light steel blue; Lg = light grey; G = grey; B = blue; Lg = light grey; Sb = steel blue; Lb = light blue; Gb = greenish blue. * RI measured by the distance method.

Gem Samples	Color (RGB)	Diaphaneity	Weight (ct)	Dimensions (mm)	Shape	Cut	RI * (Average)	Specific Density (g/cm ³)
1 left side	Lb	O	3.86	7 × 10 × 5	oval	Cabochon	1.680	3.30
2 left side	GB	O	2.91	7 × 9 × 5	trapezoidal	Cabochon	1.682	3.24
3 right side	Lsb/Lg/G	O	10.26	14 × 11 × 5	trapezoidal	Cabochon	1.681	3.28
4 right side	Lb/Lsb/Sb	O	6.30	13 × 11 × 4	oval	Cabochon	1.683	3.27
5 right side	G/Lsb/Sb	O	8.12	17 × 13 × 4	rectangular	Cabochon	1.682	3.28
6 right side	G/B/Sb/Gb	O	5.15	15 × 10 × 2	rectangular	Cabochon	1.683	3.24
7 right side	Lg/Sb/B	O	5.90	13 × 10 × 4	oval	Cabochon	1.682	3.28
8 right side	Lg/Lb	O	11.18	19 × 14 × 6	oval	Cabochon	1.680	3.26

XRPD data were collected at the Earth and Environmental Sciences Department (University of Pavia, Italy) with a Philips PW1800 (Philips, Amsterdam, The Netherlands) diffractometer with Bragg–Brentano geometry and automatic divergence slit, CuK α radiation ($\lambda = 1.5418 \text{ \AA}$, 50 kV, 30 mA) and scan speed of $1^\circ/\text{min}$, in the angular range between $2\text{--}65^\circ 2\theta$. The samples were firstly ground using an agate steel percussion mortar until they were reduced to very fine powder, and then mounted on the sample holder [19]. Qualitative and semi-quantitative analyses of the mineral phases in diopside were evaluated through the program “PANalytical XPert HighScore” (Philips, Amsterdam, The Netherlands) with an analytical error of about 5%. Rare Earth Elements (REE) and selected trace elements were determined by LA-ICP-MS analyses with a quadrupole (DRCe from Perkin-Elmer SCIEX, Waltham, MA, USA) and a 266 nm laser (Quantel Brilliant) at IGG-CNR of Pavia. Quantification was performed using SiO₂ (stoichiometric value) as internal standard and NIST SRM 610 synthetic glass as external standard. Diopside fragments were mounted in epoxy resin and polished before analyses or they were analyzed directly on rock slices (about 1mm thick). Precision and accuracy were estimated by the analyses of a BCR-2 standard and resulted better than 5 and 10%, respectively, for concentration at ppm level. LA-ICP-MS analyses were conducted both on diopside and on associated minerals.

Besides standard gemological testing, one polished rough sample was analyzed by Raman spectroscopy at the laboratories of the University of Pavia. Micro-Raman scattering measurements were conducted using a Horiba LabRam HR (Horiba Kyoto, Japan) Evolution spectrometer (holographic gratings of 600 grooves/mm) equipped with an Olympus BX41 confocal microscope at controlled temperature of 20(1) °C. Raman spectra were excited using the 532 nm line of a solid state (YAG) laser. The laser power on the sample surface was approximately 1–2 mW. The spectrometer was calibrated to the Raman peak of silicon at 520.5 cm^{-1} . Each analysis was collected for 15s over four accumulations. The spectral resolution was $\sim 2 \text{ cm}^{-1}$.

Backscattered electron (BSE) images and quantitative chemical analyses of major and minor elements were obtained with a SEM CamScan MX3000 (CAM, Beaverton, OR, USA) equipped with LaB6 at the Geoscience Department of the University of Padova, and with a JEOL JXA-8200 (JEOL, Tokyo, Japan) electron microprobe in wavelength dispersion mode (EMPA-DS) at the Department of Earth Sciences of the University of Milan. For the analyses through EMPA-DS (EDAX Inc., Mahwah, NJ, USA), the following conditions were used: 15 kV accelerating voltage, 5 nA beam current, and a count time of 60 s on peak and 30 s on the background, with a 1 μm diameter beam. Natural and synthetic minerals were used as standards: albite (Na), diopside (Ca, Mg and Si), Fe₂O₃ (Fe), orthoclase (Al and K), MnTiO₃ (Mn and Ti), Cr₂O₃ (Cr) and apatite (P). The rough data were corrected for matrix effects using a conventional Z routine in the JEOL software package (Japan Electron Optics Laboratory).

4. Results

4.1. Gemological Results

The gemological properties of eight cabochon cut diopside specimens (Figures 6–8) are listed in Table 1. The samples were fashioned from rough specimens extracted from the right (gems 3, 4, 5, 7, 8, Figure 8; gems 6, 9, Figure 6a,b) and left (gem 1 and 2, Figure 7) sides of the Sissone valley. Only cabochon 2 is totally made up of diopside and shows a very nice blue–turquoise color; the other gems consist of a more complex association made up by blue diopside with amphibole, Mg–calcite, lizardite (Table 2) which determines a more variable color from light blue to blue/greenish blue, and from light grey to grey. The diaphaneity is always opaque; all the samples are inert to long- and short-wave UV radiation. The specific density varies between 3.24 and 3.30 g/cm³; the medium refraction is in the range of 1.680–1.683. The pure diopside presents specific density between 3.22 and 3.38 and medium RI between 1.664 and 1.730 [20]. The various modal proportions of the minerals associated with diopside also contribute to the variation of the specific density and refraction indices.

Table 2. LA-ICP-MS investigations on minerals associated with diopside from the right (Table a) and left side (Table b) of the Sissone valley.

a		Forsterite						Lizardite			Phlogopite		
Element	Forst.1	Forst.2	Forst.3	Forst.4	Forst.5	Forst.6	Forst.7	Element	Liz.1	Liz.2	Element	Phl.1	Phl.2
(ppm)								(ppm)			(ppm)		
Li	3.79	6.14	12.58	11.87	7.65	16.31	14.72	Li	<2.07	<3.22	Ti	435.95	484.71
B	37.28	68.01	72.34	48.53	7.41	18.13	15.41	B	130.3	124.86	V	1446.54	1080.28
Ca	155.14	113.19	109.36	243.08	91.22	197.71	275.01	Ca	450.92	266.96	Cr	3.04	6.04
Sc	0.49	<0.31	0.94	0.48	1.07	1.36	0.61	Sc	0.99	0.55	Co	0.366	1.28
Ti	5.77	<2.33	116.07	256.87	<2.58	5.41	3.05	Ti	29.14	35.36	Ni	1.02	0.64
V	18.1	31.9	470.76	347.17	9.27	6.46	18.73	V	137.65	115.72	Zn	10.1	13.41
Cr	3.84	2.47	<4.17	<3.11	<2.88	3.37	<2.44	Cr	<1.96	<1.55	Rb	729.45	710.57
Co	0.731	0.888	0.379	0.82	1.015	1.148	0.85	Co	0.186	0.302	Sr	8.07	3.38
Ni	1.95	2.66	1.86	1.47	3.12	2.24	2.99	Ni	1.49	1.7	Y	0.069	<0.076
Zn	27.45	25.4	20.74	22.33	34.01	34.96	33.52	Zn	7.11	4.37	Zr	1.53	2.57
								Rb	0.034	0.076	Nb	1.033	1.138
								Sr	0.337	0.34	Cs	40.32	43.65
								Y	0.317	0.211	Ba	2048.01	1029.52
								Zr	0.701	0.828	Ta	0.279	0.2
								Nb	0.359	0.444	Pb	4.06	1.96
								Cs	0.0382	0.053	U	0.091	0.379
								Ba	0.182	0.222			
								La	0.89	1.032			
								Ce	1.582	1.952			
								Pr	0.195	0.222			
								Nd	0.519	0.93			
								Pb	6.78	5.2			
								Th	0.084	0.093			
								U	52.64	61.31			

b		Amphibole	
Element	Amph1	Amph2	
(ppm)			
Li	0.49	0.38	
Be	2.12	0.78	
B	5.85	4.03	
Al	2397.94	2445.56	
Sc	4.38	3.66	
Ti	123.31	116.79	
V	706.97	670.45	
Cr	8.45	4.65	
Mn	35.43	42.25	

Table 2. Cont.

a	Forsterite							Lizardite			Phlogopite			
	Element (ppm)	Forst.1	Forst.2	Forst.3	Forst.4	Forst.5	Forst.6	Forst.7	Element (ppm)	Liz.1	Liz.2	Element (ppm)	Phl.1	Phl.2
	Fe	729.5	858.38											
	Zn	7.16	7.61											
	Rb	0.2	0.34											
	Sr	7.86	7.81											
	Y	2.01	1.61											
	Zr	3.01	3.34											
	Ba	4	4.27											
	La	0.35	0.29											
	Ce	1.04	1.04											
	Nd	1.18	0.91											
	Sm	0.31	0.27											
	Eu	0.12	0											
	Gd	0.14	0.39											
	Dy	0.35	0.24											
	Er	0.23	0.14											
	Yb	0.13	0.15											

4.2. XRPD Results

The mineralogical composition of the investigated samples (Figure 9) shows remarkable variations. The blue diopside is abundant in two samples showing a vivid blue color, from both the sides of the Sissone valley (Table 3).

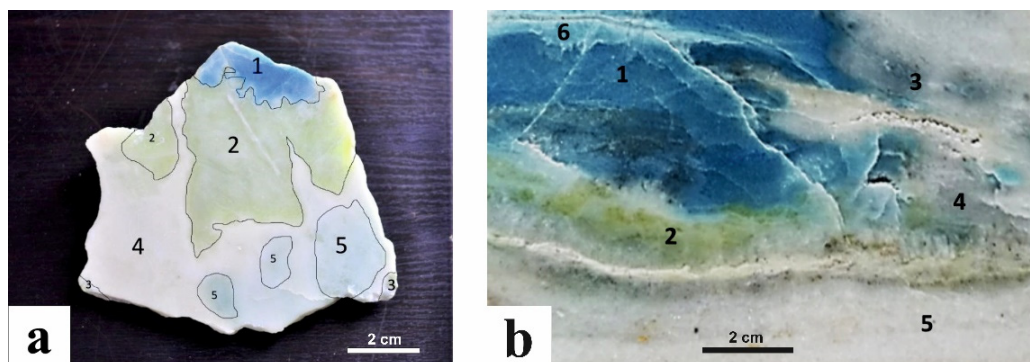


Figure 9. Marble plates used for the XRPD analyses: (a) left side, (b) right side of the Sissone valley. The different chromatic areas, with variable mineralogical composition, are evident.

The talc, which is an ubiquitous product of the diopside retrometamorphism, is present in only one sample the from the left side of the Sissone valley. The tremolite is present in all the samples from the left side but is absent in the other side. Conversely, phlogopite and forsterite are present only in the right side. Carbonate minerals consist of Mg-calcite and dolomite and are present with variable amounts in both the sides of the valley.

Table 3. Mineralogical composition of the samples from the areas 1–5 (Figure 9a,b). The semiquantitative analyses on XRPD data were performed with the program “PANalytical XPerth High Score”. Mineral name abbreviations: Di = diopside, Cal = calcite, Phl = phlogopite, Dol = dolomite, Tr = tremolite, Lz = lizardite, Fo = forsterite. [21].

	Di	Tr	Cal	Dol	Lz	Tlc	Clc	Phl	Fo
Left Side Sample	%								
A1 vivid blue	70	10	20						
A2 light olive green		20	20	20	40				
A3 grey greenish		40	40				20		
A4 milk white		5		85		10			
A5 white blue		20		40			40		
Right Side Sample	%								
A1 vivid blue	70		20				10		
A2 white grey			5	50	20			25	
A3 grey			20	10			20		50
A4 light olive green					70				30
A5 grayish green			20	10	30			40	

4.3. Optical Microscope and SEM Observations

Observations with the optical microscope and back scattered electrons-SEM (Figure 10) showed that the vivid blue portion (area 1) is characterized by a granoblastic texture forming polycrystalline aggregates (Figure 10c) in which diopside grains are equant with a quite uniform grain size (<200 μm). This type of texture results from a solid-state transformation that took place to achieve the textural equilibrium, as also demonstrated by the presence of 120° triple junctions between most of diopside grains (Figure 10c).

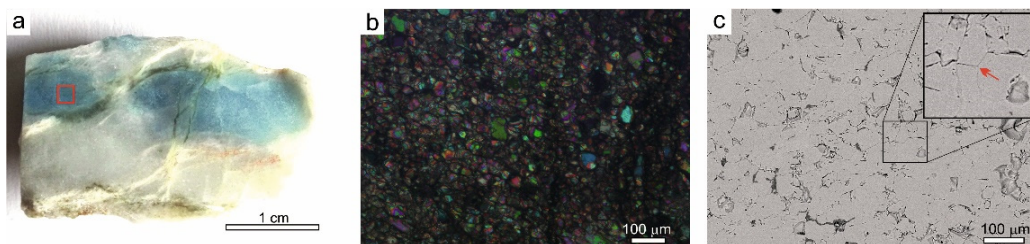


Figure 10. (a) Rock slice (right side of the Sissone valley) from which thin section was prepared. (b) Photomicrograph of the blue portion (red square in a); cross-polarized light. (c) BSE-SEM image of the same area. Some 120° triple junctions are visible among the grains (red arrows).

In Figure 11 the SEM analysis on a thick polished section containing a diopside-bearing vein in the marble is reported. SEM observations (BSE images and EDS analyses) revealed mineralogical and textural variations of the marble across the vein. In the upper part calcite contains abundant porphyroblasts of dolomite and forsterite (Figure 11b,c).

Approaching the vein, a significant reduction in the grain size without apparent changes to the mineral assemblage, except for the appearance of rare phlogopite flakes (Figure 11d), was observed. Forsterite grains may contain calcite and phlogopite inclusions (Figure 11e). The boundary between the vein and the host marble is mainly made up of lizardite and is “symmetrical”.

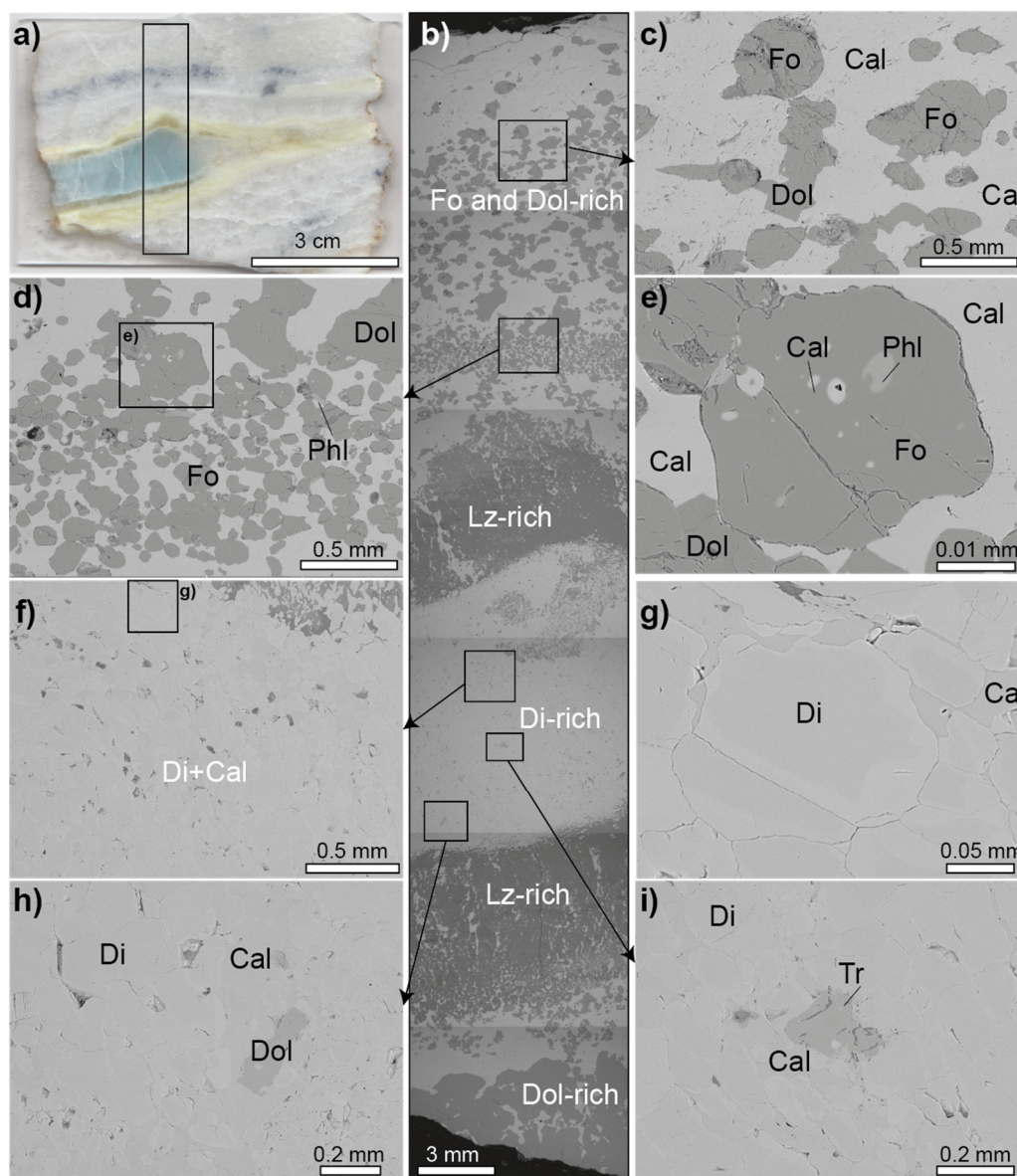


Figure 11. (a) Thick section of a sample from the right side of the Sissone valley: the rectangle is the examined portion in (b). Images (c,d,f,h,i) are magnifications highlighted in (b); image (e) is the magnification in (d) and image (g) is the magnification in (f). Mineral abbreviations: Di = Diopside; Dol= Dolomite; Fo = Forsterite; Cal = Calcite; Tr = Tremolite; Phl = Phlogopite; Lz = Lizardite [21] (photo by Antonio Langone).

The vein consists of diopside with interstitial calcite (Figure 11f,g). Diopside is chemically zoned, as revealed by a brighter rim richer in CaO (Figure 11g). Within the vein rare dolomite and tremolite grains occur. The vein termination is mostly made of dolomite, abundant phlogopite (about 1 mm across) and forsterite totally or partially replaced by lizardite and/or talc.

4.4. EMP Analyses

EMP analyses showed the most abundant elements, calculated as oxides, are SiO₂ (around 55–56 wt. %), CaO (around 25–26 wt. %) and MgO (about 18 wt. %) (Table 4), while quantities of all the other elements are very low. Among them, FeO and P₂O₅ can reach up to 0.24 and 0.22 wt. %, respectively. This composition indicates the diopside is almost pure.

Table 4. Mineral chemistry obtained through EMPA of the investigated diopsides of the lens of Figure 10a.

Oxides wt%	1	2	3	4	5	6	7
SiO ₂	56.06	55.68	55.81	56.09	56.64	55.79	55.77
TiO ₂	0.04	0.08	0.05	0.03	0.07	0.05	0.00
Al ₂ O ₃	0.03	0.02	0.03	0.04	0.04	0.04	0.02
FeO	0.14	0.12	0.09	0.13	0.12	0.12	0.24
MnO	0.02	0.00	0.00	0.02	0.08	0.00	0.01
MgO	18.34	18.13	17.84	18.15	18.49	18.37	18.54
CaO	25.91	25.75	26.07	25.51	26.29	25.79	25.81
Na ₂ O	0.00	0.06	0.02	0.02	0.02	0.00	0.05
K ₂ O	0.00	0.00	0.00	0.00	0.00	0.00	0.01
SO ₃	0.02	0.01	0.04	0.02	0.00	0.00	0.00
Cr ₂ O ₃	0.07	0.00	0.07	0.00	0.03	0.03	0.00
P ₂ O ₅	0.08	0.22	0.22	0.10	0.11	0.17	0.17
TOT	100.71	100.07	100.24	100.11	101.89	100.36	100.62
Numbers of Ions on the Basis of 6 Oxygens							
Si	2.007	2.010	2.013	2.018	2.007	2.007	2.002
Ti	0.001	0.00	0.00	0.00	0.00	0.00	0.00
Al	0.009	0.001	0.014	0.019	0.009	0.008	0.003
Fe	0.004	0.004	0.003	0.004	0.003	0.004	0.007
Mn	0.000	0.000	0.000	0.000	0.002	0.000	0.000
Mg	0.979	0.976	0.959	0.973	0.977	0.985	0.992
Ca	0.994	0.996	1.007	0.983	0.998	0.994	0.993
Na	0.000	0.004	0.001	0.001	0.001	0.000	0.003
K	0.000	0.000	0.000	0.000	0.000	0.000	0.000
Cr	0.002	0.000	0.002	0.000	0.001	0.001	0.000
TOT	3.996	3.991	3.997	3.998	3.998	3.999	3.990
Calculated End-Members							
Wo	50.26	50.31	51.12	50.10	50.35	50.13	49.73
En	49.50	49.29	48.68	49.60	49.28	49.69	49.71
Fs	0.24	0.18	0.14	0.23	0.30	0.18	0.38
Acm	0	0.21	0.07	0.07	0.07	0	0.17

Wo = wollastonite, En = enstatite, Fs = ferrosilite, Acm = acmite.

4.5. LA-ICP-MS Analyses

LA-ICP-MS investigations were conducted on samples of diopside from both the left and right sides of the valley (see Table 5). The most abundant trace elements in the samples from the left side are Fe (between 776 and 950 ppm), V (206–912 ppm), Al (38–123 ppm), Ti (13–275 ppm), Mn (64–90 ppm). Other elements present in lower amounts are Rb (0–16 ppm), Sr (1–16 ppm), Be (2–10 ppm), Cr (5–7 ppm), B (2–4 ppm), Zr (0–3 ppm). HREE are absent while LREE are very low (Table 5a).

Regarding the diopside from the right side of the valley, the most abundant elements are Fe, with contents between 430 and 638 ppm, followed by V (42–654 ppm), Mn (37–44 ppm) and Ti (8–197 ppm). Other elements in lower contents are Zn (3–9 ppm), Sr (13–25 ppm), B (4–9 ppm), Cr (2–3 ppm), Zr (1–6 ppm) (Table 5b; Figure 12).

Table 5. (a) LA-ICP-MS investigations carried out on two crystals of diopside (A and B) from area 1 of Figure 9a (left side of the Sissonevalley); (b) LA-ICP-MS investigations on blue diopside from lens of Figure 11a (right side of the Sissone valley). (*) Mn and Fe were analyzed only in the last four analysis points.

a		Diopside					
Element (ppm)	Cryst. B			Cryst. A			
	Light Zone	Dark Zone	Dark Zone	Lighter Zone	Light Zone	Dark Zone	Dark Zone
Li	1.52	5.13	9.01	0.94	2.07	7.55	2.31
Be	3.80	9.55	1.92	2.31	4.79	4.51	3.13
B	3.31	2.34	2.78	2.50	4.19	3.40	3.12
Al	112.26	38.16	75.95	91.25	122.98	39.21	67.06
Sc	2.79	2.38	1.78	1.23	2.30	2.43	3.17
Ti	18.20	219.66	274.61	27.70	12.98	163.93	140.90
V	220.28	755.89	912.10	207.92	206.77	590.25	552.18
Cr	5.36	5.02	5.30	4.89	6.78	5.06	5.24
Mn	63.95	83.99	89.80	63.86	68.01	73.25	75.65
Fe	819.29	949.32	890.39	821.50	776.18	882.19	884.45
Zn	4.30	4.13	2.33	0.97	3.06	4.59	4.29
Rb	16.24	14.70	13.97	16.25	0.06	0.00	0.07
Sr	1.66	0.80	0.68	1.63	15.20	15.37	15.77
Y	0.47	4.30	5.02	0.24	2.11	0.92	1.07
Zr	0.00	0.12	0.14	0.16	0.52	2.85	3.35
Ba	0.09	0.09	0.06	0.26	0.10	0.11	1.71
La	0.07	0.00	0.00	0.00	0.43	0.14	0.33
Ce	0.00	0.22	0.06	0.07	1.10	0.57	0.78
Nd	0.24	0.16	0.07	0.09	0.85	0.51	0.74
Sm	0.10	0.07	0.00	0.05	0.26	0.24	0.11
Eu	0.29	0.14	0.00	0.07	0.05	0.00	0.00
Gd	0.00	0.27	0.16	0.09	0.61	0.16	0.11
Dy	0.00	0.00	0.10	0.12	0.19	0.24	0.20
Er	0.52	0.54	0.57	0.62	0.09	0.15	0.14
Yb	0.05	0.03	0.07	0.00	0.06	0.12	0.310

b		Diopside														
Element (ppm)	Dark1	Dark2	Dark3	Light1	Light2	Light3	Light4	Light5	Light6	Light7	Light8	Light9	Dark4	Dark5	Dark6	Light10
B	9.4	5.48	5.22	4.97	<5.38	4.94	6.06	5.12	<4.20	<5.13	8.88	5.14	<5.32	5.09	3.78	4.9
Sc	1.08	1.27	0.96	1.04	0.97	1.05	0.96	1.29	1.2	1.36	1.04	1.19	0.76	0.72	<0.23	0.67
Ti	27.43	38.34	41.33	15.63	5.13	11.22	9.85	12.13	19.59	8.1	8.6	11.89	197.04	20	138.66	16.52
V	113.47	190.93	168.46	54.32	28.07	65.31	23.67	32.26	70.64	26.3	23.9	40.62	654.86	84.53	458.12	42.28
Cr	<2.21	3.22	<1.85	<2.15	3.38	<2.44	2.82	<2.40	2.22	<1.86	<2.22	<1.97	<2.23	<1.72	<2.05	<1.76
Mn (*)													43.58	44.27	37.43	37.88
Fe (*)													464.73	638.97	430.79	593.87
Co	0.309	0.264	0.449	0.211	0.354	0.188	0.399	0.362	0.313	0.527	0.174	0.291	0.344	0.196	0.165	0.342
Ni	<0.48	0.7	1.25	0.5	1.32	1.02	0.85	<0.45	0.78	1.36	0.5	<0.26	<0.48	0.36	1.56	<0.57
Zn	9.42	3.73	3.87	4.06	3.57	5.11	2.71	4.33	3.63	3.79	2.71	4.53	6.06	4.33	2.7	3.38
Rb	0.253	<0.047	0.048	0.051	<0.041	0.057	<0.057	0.04	<0.052	<0.039	<0.049	<0.038	<0.042	0.402	<0.030	<0.034
Sr	21.21	19.91	22.94	19.2	25.76	20.33	24.49	25.28	20.55	24.71	24.15	20.41	12.96	24.46	15.11	21.93
Y	1.079	0.359	0.681	0.639	0.714	0.963	0.66	0.575	0.893	0.694	0.737	0.706	0.318	1.291	0.223	0.951
Zr	0.609	1.4	1.062	0.586	0.304	0.723	0.479	0.341	0.773	0.574	0.455	0.782	5.49	1.069	3.41	0.712
Nb	0.033	<0.026	0.022	<0.0223	<0.023	<0.025	<0.0195	<0.031	0.065	<0.029	<0.030	<0.028	0.057	<0.036	<0.032	0.043
Cs	0.06	0.0306	0.0152	0.027	0.0229	<0.0143	0.0143	0.0186	<0.0218	<0.0161	0.0246	<0.0155	<0.0099	0.075	<0.0137	<0.0183
Ba	1.915	0.458	0.304	0.037	0.087	0.074	0.335	0.106	0.147	<0.019	0.159	<0.0192	<0.019	1.053	0.025	0.042
La	0.985	0.868	1.029	0.343	0.558	0.464	0.476	0.748	0.921	0.642	0.701	0.493	0.106	0.944	0.26	0.607

Table 5. Cont.

Element (ppm)	Diopside															
	Dark1	Dark2	Dark3	Light1	Light2	Light3	Light4	Light5	Light6	Light7	Light8	Light9	Dark4	Dark5	Dark6	Light10
Ce	2.29	2.09	2.19	1.733	1.803	1.523	1.659	1.913	2.2	2.04	1.784	1.576	0.435	2.38	0.579	1.624
Pr	0.273	0.252	0.283	0.303	0.244	0.188	0.208	0.256	0.311	0.305	0.3	0.2	0.102	0.26	0.074	0.286
Nd	1.04	0.76	1.54	0.94	0.77	0.89	0.96	1.17	1.12	0.93	1.06	0.513	0.45	1.25	0.29	1.16
Sm	0.247	0.317	0.133	0.214	0.365	0.231	<0.145	<0.171	0.175	0.121	0.122	<0.129	<0.102	0.193	<0.100	<0.115
Eu	0.092	<0.043	<0.032	0.057	0.056	<0.029	<0.031	0.045	0.055	<0.033	<0.029	<0.034	<0.034	<0.022	<0.038	0.029
Gd	0.171	<0.135	0.142	0.132	0.155	0.211	<0.142	0.088	0.134	<0.085	0.118	0.294	0.18	<0.134	<0.054	0.318
Tb	<0.0156	<0.0160	<0.020	0.0231	0.0246	<0.0218	<0.0167	<0.0108	0.0346	0.0217	0.0261	<0.0129	0.02	0.021	<0.0078	<0.0200
Dy	0.214	<0.098	0.114	0.183	<0.121	0.186	<0.073	<0.066	0.086	<0.093	0.231	0.1	<0.086	0.185	<0.034	0.148
Ho	<0.026	0.0428	0.0126	0.0286	0.025	<0.024	0.0217	0.0262	<0.021	0.012	0.049	0.0297	0.02	0.0249	<0.0147	0.0193
Er	<0.086	0.077	0.171	<0.046	<0.067	0.13	<0.056	0.061	0.141	0.126	<0.086	<0.071	<0.066	<0.100	<0.083	<0.060
Tm	0.0108	0.0303	<0.0184	0.0196	<0.0152	0.0332	<0.0182	0.0197	0.0214	<0.0134	<0.0139	<0.0183	<0.0149	<0.0192	0.0097	0.0165
Yb	<0.106	<0.134	0.218	0.103	<0.165	<0.149	<0.081	0.177	0.101	<0.120	<0.062	0.106	0.088	<0.109	0.061	<0.086
Lu	<0.021	<0.0185	0.0284	<0.0248	<0.036	<0.0179	<0.0194	<0.0125	<0.0157	0.018	0.0196	<0.0173	<0.0225	0.018	<0.0127	<0.029
Hf	0.083	0.091	<0.085	<0.093	<0.157	0.82	<0.149	<0.061	0.93	<0.069	<0.114	<0.060	0.27	<0.062	0.58	0.062
Ta	<0.0208	<0.0214	<0.0102	<0.0181	<0.046	0.0243	<0.028	0.0149	<0.0259	<0.0117	0.023	0.0154	<0.00	<0.0109	0.012	<0.0246
Pb	1.94	6.39	0.569	3.54	0.871	0.65	0.494	1.025	6.89	0.769	0.64	0.769	0.92	2.65	1.03	0.684
Th	<0.023	0.209	0.088	<0.0209	0.038	0.0155	0.0382	0.034	0.063	<0.0190	<0.0114	<0.0189	0.11	0.023	<0.00	<0.026
U	0.441	3.03	1.624	0.842	0.093	0.892	0.125	1.452	1.274	0.032	0.058	0.0503	0.125	1.695	0.048	0.067

In general, the contents of each element show large variations but the ranges in the diopside from the right side of the valley are comparable to those from the left. Elements such as Na and K are not present. Rb, which is much more abundant in the samples from the left side (crystal b, 14–16 ppm), shows the most apparent differences between diopside grains from the two sides of the valley. It is interesting to note that for both sides a positive correlation was observed for V and Ti (Figure 12), Mn and Fe, and Ce and La. An opposite trend was observed for Rb and Sr.

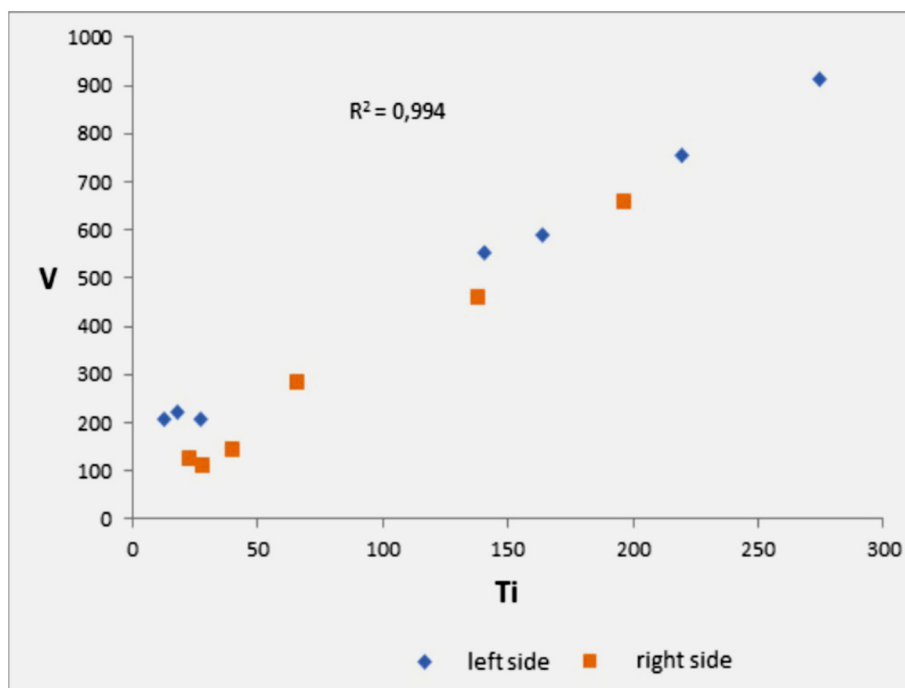


Figure 12. Correlations of V vs. Ti contents (ppm) from LA-ICP-MS analyses in the blue diopside from the left and right sides of the Sissone valley.

Regarding the chromophore elements, V and Ti are more abundant in the darker diopside grains than in the lighter ones. Fe is another important chromophore, which is abundant in all the samples but prevails in the dark ones. Conversely, the Mn content is not related to the blue tint, which appears to be mainly controlled by V, Ti and, to a lesser extent, Fe.

LA-ICP-MS analyses were also performed on two spots of a crystal composed by an association of pyroxene and amphibole, which shows a dark blue color (see Table 5b). These spots feature much higher Al contents (around 2400 ppm) which is obviously related to amphibole, and also lower Mn, some Ba (around 4 ppm) and no Li with respect to the other parts, while the other trace elements do not show relevant variations. In this case, the higher vanadium contents also determine the dark blue color.

4.6. Raman Analyses

Figure 13a shows the locations of spots with different colors in a vein in the marble of the right side, investigated by Raman spectroscopy; the analyses were performed in order to determine the presence of diopside and associated minerals. The spots showed a different mineralogical composition: diopside (points 1 and 2); lizardite (points 3 and 4); Mg-calcite (point 5); tremolite (point 6); dolomite (point 7) and forsterite (point 8), as also found by XRPD investigation. The Raman spectra of pyroxene are characterized by four types of vibration bands: (1) Si-O non bridging stretching (Si-O_{nbr}); (2) Si-O bridging stretching (Si-O_{br}); (3) O-Si-O bending; and (4) cation M1, M2-oxygen vibration modes (M-O). The Si_{nbr} stretching modes are present in the spectra at frequencies higher than the Si-O_{br} modes, due to a stronger constant force, i.e., the coefficient that links the displacement of the atoms from their equilibrium position with the force that this displacement induces in the adjacent atoms (in the case of Si-O_{br} bonds, the force constant is shared between the adjacent tetrahedra) [22–28].

The spectra of the diopside from the Sissone valley are characterized by two intense bands corresponding to the Si-O_{nbr} stretching mode (1012 cm^{-1}) and to the stretching of Si-O_{br} bonds ($664\text{--}666\text{ cm}^{-1}$) (Figure 13b; Table 6). In the $500\text{--}560\text{ cm}^{-1}$ region there are bands assigned to the O-Si-O bending modes and in the lower wavenumber region the observed bands are due to the cation-oxygen vibrations (M-O).

In Figure 13c a rough sample of marble with blue diopside from the left side of the valley is reported. According to Raman analyses, blue diopside and tremolite in this sample show the typical absorption band of calcite at about 1089 cm^{-1} : this would indicate that the grains of the two minerals are very small and closely interspersed with calcite crystals. The analyses also revealed the presence of dolomite and forsterite. Table 6 shows the absorption bands of the minerals associated with blue diopside: Table 6a represents the paragenesis of the vein from the right side of the valley, while 6b represents that from the left side (Figure 14) [27–34].

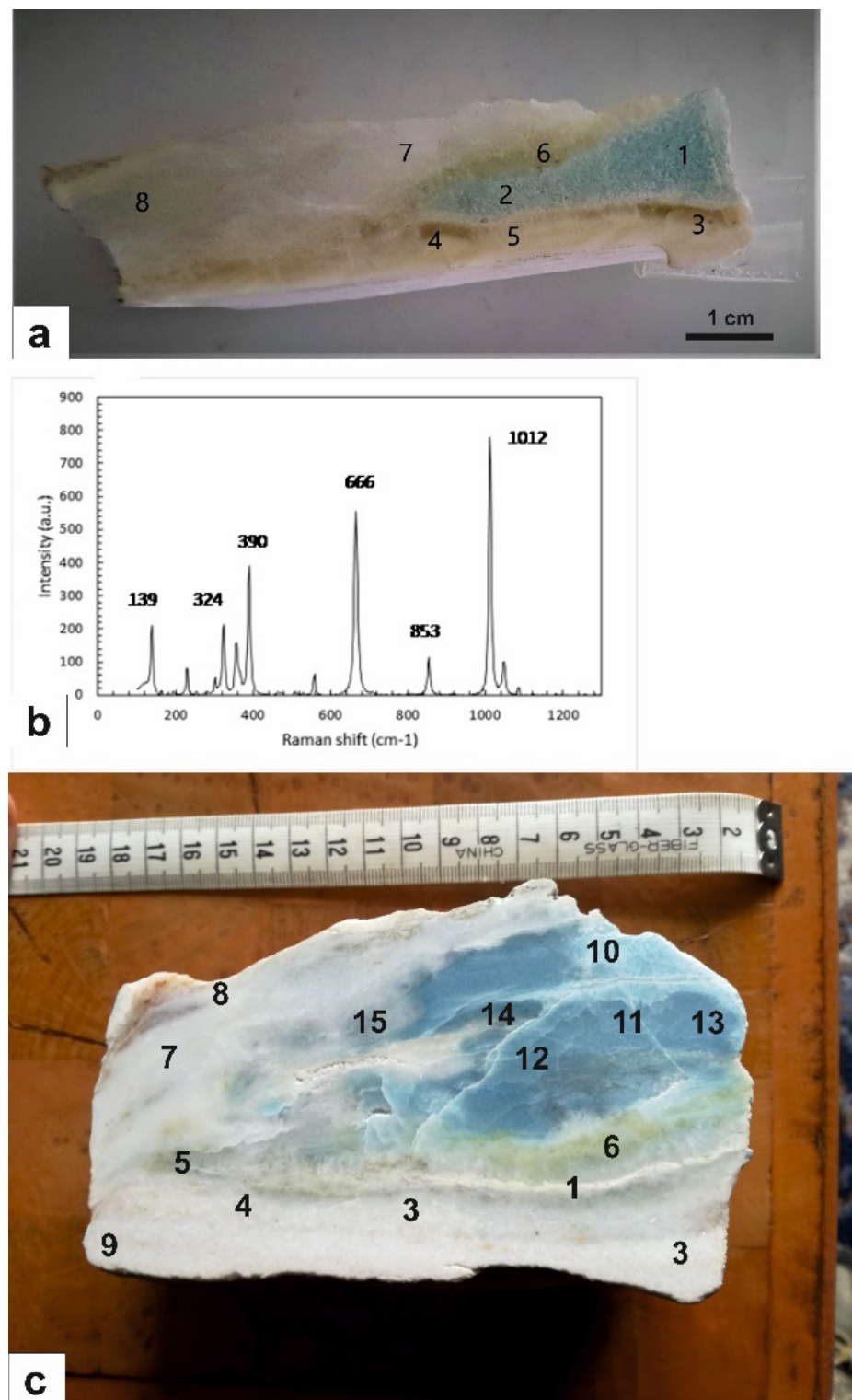


Figure 13. (a) Sample from the right side of the valley, showing the points analyzed by Raman spectroscopy: points 1 and 2 = diopside; points 3, 4 and 6 = lizardite; point 5 = calcite; points 7 and 8 = forsterite; (b) Raman spectrum of the studied diopside; (c) sample from the left side with the analyzed points: point 1 = dolomite; points 2, 3, 4, 7, 8, 9, 15 = calcite; points 10, 11, 12, 13 = diopside; point 14 = tremolite; point 5 = forsterite; point 6 = lizardite.

Table 6. Raman analyses on the mineral phases occurring in the diopside-bearing marbles; the band numbers and their assignments are reported: (Table a) right and (Table b) left side of the Sissone valley. At about 1089 cm^{-1} the typical absorption band of calcite is present.

a		Diopside [27]	
230, 285	230, 285		M-O stretching/bending
324	324		M-O stretching/bending
358	360		M-O stretching/bending
390	390		M-O stretching/bending
559	560		O-Si-O bending
666	664		Si-O _{br} stretching
853, 1012, 1050	853, 1012, 1050		Si-O _{nbr} stretching
1089 *			* CO ₃ symmetric O-C-O stretching
Lizardite [29]			
—, 280	228, 280	227, 280	O-OH-O vibration groups
350, 382	350, 382	349, 383	SiO ₄ tetrahedra bending vibrations
430	430	430	Mg-OH antisymmetric translation
620	228	620	Hydroxyl groups vibrations; OH-Mg-OH translation
690	693	692	Si-O _{br} -Si symmetric stretching mode groups
1100	1100	1100	Si-O groups antisymmetric stretching modes
Calcite [30]			
	156		Ca/CO ₃ translation mode
	279		Ca/CO ₃ translation mode
	711		Symmetric CO ₃ deformation mode
	888, 1087		Symmetric CO ₃ stretching mode
Forsterite [31,32]			
302	302		M2 translation
481	481		SiO ₄ symmetric bending
560	560		SiO ₄ rotation
623	623		SiO ₄ asymmetric stretching
823	823		Si-O symmetric stretching
856	856		Si-O asymmetric stretching
953	955		Si-O asymmetric bending
1100	1098		Si-O asymmetric bending

Table 6. Cont.

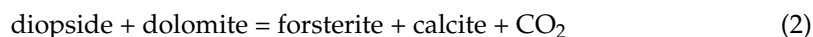
b		Diopside [27]
230	232	M-O stretching/bending
286, 326, 358	284, 326, 359	M-O stretching/bending
390	391	M-O stretching/bending
560	560	O-Si-O bending
666	666	Si-O _{br} stretching
855, 1013, 1050	856, 1013, 1051	Si-O _{nbr} stretching
1089	1088*	CO ₃ symmetric O-C-O stretching
		Lizardite [29]
228, 280	227, 279	O-OH-O vibration groups
349, 382	350, 383	SiO ₄ tetrahedra bending vibrations
430	431	antisymmetric Mg-OH anti translation
620	620	vibration of the hydroxyl of the layers; OH-Mg-OH translation mode
692	693	Si-O _{br} -Si symmetric stretching mode groups
1098	1100	antisymmetric stretching modes (ν_{as}) of Si-O groups
		Dolomite [33]
176, 301		Ca, Mg-CO ₃ translation mode
724		M-O out-of-plane bending mode
880, 1099		CO ₃ symmetric stretching
		Forsterite [31,32]
306		M2 translation
476		SiO ₄ in plane bending
557		SiO ₄ rotation mode
623		SiO ₄ asymmetric stretching
826		Si-O symmetric stretching
855, 953		Si-O asymmetric stretching
1096		Si-O out-of-plane bending
		Tremolite [34]
123, 180		Lattice vibration mode
352, 416		M-OH translation mode
586		Si ₄ O ₁₁ deformation mode
678, 743		Si-O-Si symmetric stretching
932		O-Si-O symmetric stretching



Figure 14. A 1.32 mm assemblage of green lizardite crystals from Sissone valley. (Collection of Domenico Preite, photo by Matteo Chinellato).

5. Discussion and Conclusions

The marbles from the Sissone valley contain reaction veins linked to a regional fracture system which probably formed during the cooling and uplift of Masino-Bregaglia pluton [35]. The mineral assemblages found in individual zones of these veins are the following: calcite + forsterite + dolomite, calcite + diopside, calcite + tremolite, calcite + lizardite, calcite + talc. The vein types analyzed in this work are: (1) compositionally zoned pinch and swell lenses (up to 20 cm thick), made up by finely granular blue–turquoise to colorless diopside and Mg-calcite, surrounded by fibrous tremolite and green diopside [36,37]; (2) centimetric blue diopside patches (up to 60 cm), greenish-grey forsterite, green lizardite and dark blue phlogopite [36,37]; (3) thin elongated veins made up of dark blue forsterite and milk white dolomite.



From the last reaction, the formation of forsterite requires the infiltration into marble of silica dissolved in aqueous fluids. Additionally, some phase equilibrium studies suggested that when a fluid is saturated with quartz, most of the silica in the fluid phase is removed through reaction (4) resulting in the formation of diopside



and then forsterite forms by Reaction (3). Reactions (1) and (2), instead, do not need an additional source of silica such as the infiltration of silica-rich aqueous fluids.

The EMP analyses of the main elements have established that the blue pyroxene of the Sissone valley can be classified as almost pure diopside; the omphacitic component, present in the “violane” from the Praborna mine in Italy [7], is absent in this case.

The XRPD and Raman analyses showed the mineralogical association of the diopside-bearing rock is made up by Mg-calcite, phlogopite, lizardite, clinocllore, dolomite, forsterite and rare tremolite; this composition is in agreement with the literature [15].

Microscope observations highlighted that diopside has a polycrystalline texture and the crystals of this mineral are bound together by grains composed of Mg calcite, as revealed by Raman Spectroscopy. The diopside from Sissone valley shows a beautiful blue color, sometimes blue and white. The blue–turquoise hue is due to chromophore elements such as V, Ti and, to a lesser extent, Fe and Mn, while the white color can be attributed to the previously described white interstitial magnesian calcite grains.

The minerals associated with diopside in the lenticular veins (tremolite, lizardite, forsterite, phlogopite) also show enrichments in V. Tremolite from the left side of the valley, which has a blue color, while it varies from colorless to pale green in the samples from the right slope.

Vanadium is also an important chromophore element in other precious gems: together with Cr³⁺ it gives a velvety green color to the emerald, a pink–orange color to the Padparasha variety of corundum and the blue color to tanzanite, a rare variety of zoisite extracted only from the Merelani deposit in Tanzania [38,39]. Fe, Ti and V rich-minerals are found in mafic–ultramafic rocks of the Kola region in Siberia [40], in the stratified intrusion of Bushveld in South Africa, [41] and in the giant deposits of the Panzhihua region (SW China) [42]. In these ores, V is found mainly in oxides such as spinel.

In the diopside-bearing marble from Sissone valley, V and Cr could derive from the carbonation processes of peridotites, as these elements are abundant in ultramafic rocks. The Malenco ultramafic body is a large serpentized mantle portion of subcontinental origin that was affected by contact metamorphism during the emplacement of Masino-Bregaglia intrusion. Contact metamorphism resulted in the formation of a < 10 m thick lenses of metacarbonate rocks [43] due to the influx of a hydrothermal fluid that reacted with the serpentinite [44]. Prograde metamorphism produced de-serpentinization and formation of fluids as suggested by [45] on the basis of fluid inclusion investigation. It is therefore likely that V- and Cr-rich fluids derived from ultramafic rocks were present in this area during contact metamorphism.

A comparison with other worldwide diopsides with similar properties was also performed. Blue diopside with polycrystalline texture has been found in three locations in Russia: the first in the Khakassia region of Eastern Siberia [46,47], while the second and third are near Lake Baikal [48,49]. Another type of diopside with similar properties is the aforementioned “violane”, which is extracted from the Praborna mine in the Aosta Valley, Italy [7]. The “violane” is also polycrystalline but, unlike the diopside of the Sissone valley, the color is markedly purple with some shades of blue; the chromophore elements are represented by Mn and Fe, while V is practically absent. Another noteworthy type is the blue diopside of Baffin Island in Canada [50], erroneously defined as “violane”. The color of the Baffin Island diopside is not purple but blue due to a Fe²⁺-Ti⁴⁺ charge-transfer reaction, such as that which occurs in the blue variety of corundum.

Another V-rich variety of diopside is lavrovite, with the hypothetical formula Ca(Mg,V)Si₂O₆; its color is mainly emerald green but also blue, bluish and violet; it is found in the magnesian skarns in the Lake Baikal area in Russia [20].

The beautiful blue color diopside from Sissone valley is highly prized as a collectible mineral. This mineral is locally well known: the master sculptor Silvio Gaggi used the white marble with blue veins to create a beautiful Madonnina statue in the town of Chiesa Valmalenco (Sondrio province, Italy; Figure 15).

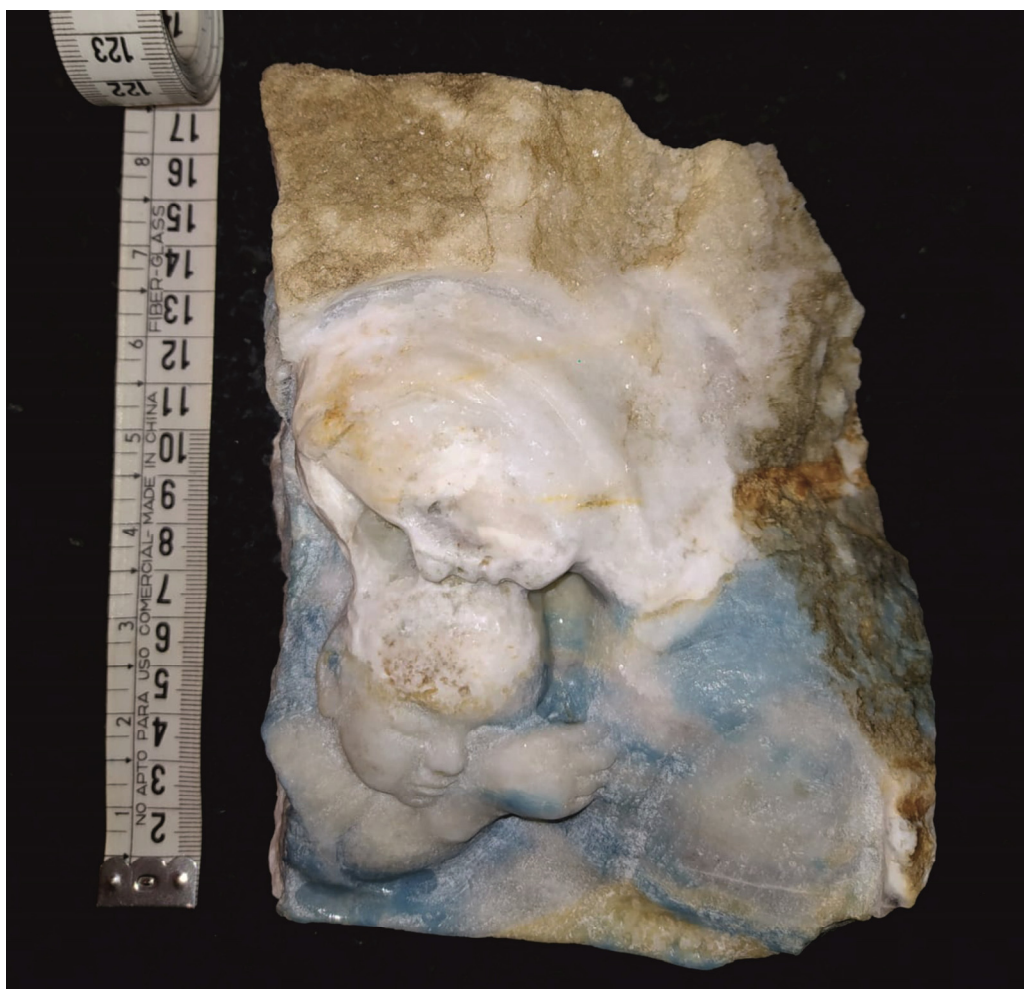


Figure 15. Statue of the Madonna sculpted by the artist Silvio Gaggi (Chiesa Valmalenco) using marble with blue diopside from Sissone valley.

Gemological cutting and polishing of this mineral are possible but with some problems, as the diopside crystals are “cemented” by calcite granules with different hardness and competence. These structural characteristics make the raw samples being processed more fragile, because during the cutting operations microcracks and crushing can be generated. Despite these drawbacks, the portions with an intense blue color, richer in chromophore V^{4+} , are also cut into cabochon and used for the preparation of jewelry, especially necklaces and pendants that are less affected by problems due to the different mechanical characteristics of the mineral phases.

The blue diopside of the Sissone Valley presents good opportunities for commercial diffusion, especially in neighboring areas such as the province of Sondrio or more generally in Northern Italy. Wider commercialization is hampered not so much by the scarce availability of the mineral in the original outcrops but rather by logistical reasons: in fact, it is difficult to reach the richest areas containing this mineral, as they are located at high altitudes and connected to the valley floor by narrow paths, for the most part only walkable.

Author Contributions: Conceptualization, F.C., M.S., L.M., I.F. and M.V.; methodology, F.C., L.M., M.G., A.L., M.V.; validation, all the authors; formal analysis, F.C., M.G., A.L., O.B.; investigation, all the authors; data curation, F.C., M.S.; writing—original draft preparation, F.C., M.S., L.M.; writing—review and editing, F.C., M.S.; supervision, F.C. All authors have read and agreed to the published version of the manuscript.

Funding: This research received no external funding.

Data Availability Statement: not applicable.

Acknowledgments: The authors are grateful to Enrico Borghi and Alessandro Focchi for cabochon photos, Pietro Nana for diopside samples, Matteo Chinellato for lizardite photo, Federico Spaggiari for help during the geological field trip.

Conflicts of Interest: The authors declare no conflict of interest.

References

1. Schumann, W. *Gemstones of the World*; Sterling Publishing: New York, NY, USA; London, UK, 2007; p. 190.
2. Anthony, J.W.; Bideaux, R.A.; Bladh, K.W.; Nichols, M.C. *Handbook of Mineralogy*; Mineralogical Society of America: Chantilly, VA, USA, 2003. Available online: <http://www.handbookofmineralogy.org/> (accessed on 20 May 2021).
3. Thomas, A. *Gemstones: Properties, Identification and Use*; New Holland Publishers (UK) Ltd.: London, UK, 2009; p. 151.
4. Zhang, Z.C.; Mahoney, J.J.; Mao, J.W.; Wang, F.S. Geochemistry of picritic and associated basalt flows of the western Emeishan flood basalt province, China. *J. Petrol.* **2006**, *47*, 1997–2019. [[CrossRef](#)]
5. Zhang, Z.C.; Mao, J.W.; Cai, J.H.; Kusky, T.; Zhou, G.; Yan, S.H.; Zhao, L. Geochemistry of picrites and associated lavas of a Devonian island arc in the Northern Junggar terrane, Xinjiang (NW China), implications for petrogenesis, arc mantle sources and tectonic setting. *Lithos* **2008**, *105*, 379–395. [[CrossRef](#)]
6. Lazarelli, H.N. *Blue Chart Gem Identification*; Gemmarum Lapidator: Cavalese, Italy, 2010; p. 54.
7. Diella, V.; Bocchio, R.; Caucia, F.; Marinoni, N.; Langone, A.; Possenti, E. New insights for gem-quality Mn-bearing diopside-omphacite, violane variety, from Saint Marcel (Val D'Aosta, Italy): Its trace elements and spectroscopic characterization. *Minerals* **2021**, *11*, 171. [[CrossRef](#)]
8. Trommsdorff, V.; Piccardo, G.B.; Montrasio, A. From magmatism through metamorphism to sea floor emplacement of subcontinental Adria lithosphere during pre-Alpine rifting (Malenco, Italy). *Schweiz. Mineral. Petrogr. Mitt.* **1993**, *73*, 191–203.
9. Hermann, J.; Müntener, O.; Trommsdorff, V.; Hansmann, W.; Piccardo, G.B. Fossil crust to mantle transition, Val Malenco (Italian Alps). *J. Geophys. Res.* **1997**, *102*, 20123–20132. [[CrossRef](#)]
10. Hermann, J.; Müntener, O.; Günther, D. Differentiation of mafic magma in a continental crust to-mantle transition zone. *J. Petrol.* **2001**, *42*, 189–206. [[CrossRef](#)]
11. Sciesa, E. Geologia delle Alpi Centrali lungo la traversa Colico-Passo dello Spluga (Province di Sondrio e Como). *IL Nat. Valtellin.* **1991**, *2*, 3–34.
12. Condlife, E.; Mottana, A. Esperimenti sul Ghiandone del massiccio della Val Masino- Bregaglia tra 1 e 3 KB P(H₂O). *Rend. Soc. Ital. Miner. Petrol.* **1976**, *XXXII*, 71–81.
13. Bedognè, F.; Montrasio, A.; Sciesa, E.E. Le rocce intrusive Terziarie, F. L'aureola di contatto, G. Le concentrazioni metallifere ed i filoni di quarzo. In *I Minerali della Provincia di Sondrio, Valmalenco*; Tipografia Bettini: Sondrio, Italy, 1993; pp. 133–212.
14. Montrasio, A.; Trommsdorff, V.; Hermann, J.; Müntener, O.; Spillmann, P. Carta Geologica della Valmalenco (scala 1:25.000). In *Quaderni di Geodinamica Alpina e Quaternaria*; Central Poligrafico: Milan, Italy, 2004.
15. Wenk, R.; Maurizio, R. Geological observation in the Bergell Area (SE-Alps), II. Contact Minerals from Mt. Sissone-Cima di Vazzeda (A Mineralogical Note). *Schweiz. Mineral. Petrogr. Mitt.* **1970**, *68*, 133–140.
16. Bucher-Nurminen, K. The formation of metasomatic reaction veins in dolomitic marble roof pendants in the Bergell Intrusion (Province Sondrio, Northern Italy). *Am. J. Sci.* **1981**, *281*, 1197–1222. [[CrossRef](#)]
17. Bucher, K. Growth mechanisms of metasomatic reaction veins in dolomite marbles from the Bergell Alps. *Miner. Petrol.* **1998**, *63*, 151–171. [[CrossRef](#)]
18. Vanotti, M. Ritrovamento di Diopside Blu nei Marmi della Val Sissone. Master's Degree Thesis, Università degli Studi di Pavia, Milan, Italy, 2014, unpublished.
19. Moore, D.M.; Reynolds, R.C., Jr. *X-ray Diffraction and the Identification and Analysis of Clay Minerals*, 2nd ed.; Oxford University Press: New York, NY, USA, 1997.
20. Available online: www.mindat.org (accessed on 15 August 2020).
21. Whitney, D.L.; Evans, B.W. Abbreviations for names of rock-forming minerals. *Am. Mineral.* **2010**, *95*, 185–187. [[CrossRef](#)]
22. Mc Millan, P. Structural studies of silicate glasses and melts-applications and limitations of Raman spectroscopy. *Am. Mineral.* **1984**, *69*, 622–644.
23. Mernagh, T.P.; Hoatson, D.M. Raman Spectroscopic Study of Pyroxene Structures from the Munnimunni Layered Intrusion, Western Australia. *J. Raman Spectr.* **1997**, *28*, 647–658. [[CrossRef](#)]
24. Huang, E.; Chen, C.H.; Huang, T.; Lin, E.H.; Xu, J. Raman spectroscopic characteristics of Mg-Fe-Ca pyroxenes. *Am. Mineral.* **2000**, *85*, 473–479. [[CrossRef](#)]
25. Downs, R.T. The RRUFF Project: An integrated study of the chemistry, crystallography, Raman and infrared spectroscopy of minerals. In Proceedings of the 19th General Meeting of the International Mineralogical Association, Kobe, Japan, 23–28 July 2006; Available online: www.ruff.info (accessed on 20 December 2020).

26. Katerinopoulou, A.; Musso, M.; Amthauer, G. A Raman spectroscopic study of the phase transition in omphacite. *Vib. Spectr.* **2007**, *48*, 163–167. [[CrossRef](#)]
27. Buzatu, A.; Buzgar, N. The Raman study of single-chain silicates. *Analele Științifice Universitatii Al. I. Cuza Iași Geologie* **2010**, *LVI*, 1.
28. Hanneman, W. *Pragmatic Spectroscopy for Gemologists*; Hanneman Gemological Instruments: Tucson, Arizona, 2011; p. 29.
29. Rinaudo, C.; Gastaldi, D.; Belluso, E. Characterization of chrysotile, antigorite and lizardite by FT-Raman spectroscopy. *Canad. Miner.* **2003**, *41*, 883–890. [[CrossRef](#)]
30. Gunasercaran, S.; Anbalagan, G.; Pandi, S. Raman and Infrared spectra of carbonates of calcite structure. *J. Raman Spectr.* **2006**, *37*, 892–899. [[CrossRef](#)]
31. Chopelas, A. Single crystal Raman spectra of forsterite, fayalite and monticellite. *Am. Miner.* **1991**, *76*, 1101–1109.
32. Kolesov, B.A.; Geiger, C.A. A Raman spectroscopy study of Fe-Mg olivines. *Phys. Chem. Miner.* **2004**, *91*, 142–154. [[CrossRef](#)]
33. Farsang, S.; Facq, S.; Redfern, S.A. Raman modes of carbonate minerals as pressure and temperature gauges up to 6 GPa and 500 °C. *Am. Miner.* **2018**, *103*, 1988–1998.
34. Apopei, I.A.; Buzgar, N. The Raman study of amphiboles. *Analele Științifice Universitatii Al. I. Cuza Iași Geologie* **2010**, *LVI*, 57–84.
35. Müntener, O.; Baumgartner, L.; Reusser, E. Day 2: Metasomatic veins. In Proceedings of the Goldschmidt Conference 2009 Field Trip, Barcelona, Spain, 27–29 June 2009; pp. 27–37.
36. Ferry, J.M.; Ushikubo, T.; Valley, J.W. Formation of forsterite by silicification of dolomite during contact metamorphism. *J. Petrol.* **2011**, *52*, 1619–1640. [[CrossRef](#)]
37. Müller, T.; Baumgartner, L.P.; Foster, C.T.J.; Vennemann, T.W. Metastable prograde mineral reactions in contact aureoles. *Geology* **2004**, *32*, 821–824. [[CrossRef](#)]
38. Bocchio, R.; Adamo, A.; Bordoni, V.; Caucia, F. Gem-quality zoisite from Merelani (Northeast Tanzania): Review and new data. *Per. Mineral.* **2012**, *81*, 379–391.
39. Fischer, R.P. Vanadium resources in Titaniferous Magnetite deposits. *Geol. Resour. Vanadium Depos.* **1973**, *926*, 18.
40. Kompanchenko, A.A.; Voloshin, A.V.; Balagansky, V.V. Vanadium Mineralization in the Kola Region, Fennoscandian Shield. *Minerals* **2018**, *8*, 474–494. [[CrossRef](#)]
41. Harne, D.M.W.; Von Gruenewaldt, G. Ore-forming processes in the upper part of the Bushveld complex, South Africa. *J. Afric. Earth Sci.* **1995**, *20*, 77–89. [[CrossRef](#)]
42. Zhang, Z.C.; Mao, J.W.; Saunders, A.D.; Ai, Y.; Li, Y.; Zhao, L. Petrogenetic modeling of three mafic-ultramafic layered intrusions in the Emeishan large igneous province, SW China, based on isotopic and bulk chemical constraints. *Lithos* **2009**, *113*, 369–392. [[CrossRef](#)]
43. Trommsdorf, V.; Connelly, J.A.D. The ultramafic contact aureole about Bregaglia (Bergell) tonalite: Isograds and a thermal model. *Schweiz. Mineral. Petrogr. Mitt.* **1992**, *76*, 537–546.
44. Trommsdorf, V.; Evans, B.W. Antigorite-ophicarbonates: Contact Metamorphism in Valmalenco, Italy. *Contrib. Mineral. Petrol.* **1977**, *62*, 301–312. [[CrossRef](#)]
45. Peretti, A.; Dubessy, J.; Mnlis, J.; Frost, B.R.; Trommsdorff, V. Highly reducing conditions during Alpine metamorphism of the Malenco peridotite (Sondrio, northern Italy) indicated by mineral paragenesis and H₂ in fluid inclusions. *Contrib. Mineral. Petrol.* **1992**, *112*, 329–340. [[CrossRef](#)]
46. Shil'tsina, A.D.; Vereshchagin, V.I. Ceramic tiles containing diopside and clay raw material from Khakassia. *Glass Ceram.* **2000**, *57*, 87–90. [[CrossRef](#)]
47. Laurs, B. Blue diopside from Russia. *J. Gemm.* **2020**, *37*, 124–126.
48. Zadov, A.E.; Pertsev, N.N.; Belakovsky, D.I.; Chukarov, N.V.; Kuznetsova, O.Y. Foshagite and hillebrandite from skarn xenoliths of ioko-Dovyrensky massif. *Proceed. Russ. Mineral. Soc.* **2004**, *133*, 73–83, (In Russian with English Abstract).
49. Simakin, A.G.; Kislov, E.V.; Salova, T.P.; Shaposhnikova, O.Y.; Nekrasov, A.N. Reduced CO₂ Fluid as an Agent of Ore-Forming Processes: A Case Study of Dolomite-Replacement Skarns at the Yoko-Dovyren Massif. *Petrology* **2019**, *27*, 1–16. [[CrossRef](#)]
50. Herd, C.D.K.; Peterson, R.C.; Rossman, G.R. Violet-colored diopside from southern Baffin Island, Nunavut, Canada. *Canad. Miner.* **2000**, *38*, 1193–1199. [[CrossRef](#)]